Adaptive Grid Embedding Navier-Stokes Technique for Cascade Flows

Roger L. Davis* and John F. Dannenhoffer III*
United Technologies Research Center, East Hartford, Connecticut 06108

A new two-dimensional adaptive grid embedding technique for the efficient and accurate calculation of the Navier-Stokes equations is presented. This procedure represents a combination of the adaptive Euler procedure developed by Dannenhoffer and Baron and the cascade viscous flow analysis of Davis et al. Steady-state solutions are computed using an explicit, finite-volume, time marching technique in which global and embedded meshes are coupled via a multiple-grid algorithm. Solutions are presented for inviscid as well as turbulent viscous flows through quasi-three-dimensional turbomachinery cascades, demonstrating that the current procedure can accurately and efficiently track complex flows with multiple length scale phenomena such as shocks, separated flows, shock/boundary-layer interactions, trailing edge base flows, and wakes. These results show the merit of using an "intelligent" grid system within a Navier-Stokes solution procedure, which automatically refines the computational grid around flow features to obtain grid independent solutions and eliminate user interaction and corresponding multiple-pass calculations. In addition, these results show that the current Navier-Stokes technique provides an adequate model of the physics of complex turbomachinery flows.

Introduction

ONE of the most difficult problems faced by the developers of computational simulations of the Euler and Navier-Stokes equations is the tradeoff between fine grids for high accuracy and coarse grids for high efficiency. Fortunately, in most flowfields, the computational errors associated with rapid solution variations (and, hence, the truncation errors) are not uniformly distributed over the domain, but are instead concentrated at a few isolated nonsmooth flow features, such as shock waves and viscous layers. Hence, if one concentrates the computational grid, and, therefore, effort, at these features, it is possible to achieve high accuracy and efficiency simultaneously; this is the basis of a whole class of techniques known as adaptive grid methods.

The computation of flows about very complex configurations, especially in three-dimensional domains, can also be simplified in terms of grid generation through the use of unstructured or semistructured grids. Researchers,[1-6] using finite-difference and control volume techniques, have recently moved towards unstructured grid systems to compute flows over complex two- and three-dimensional geometries. Unstructured grid solution procedures offer great potential in solving many complicated flow problems in turbomachinery, such as flows in rotor tip clearance regions, combustors, disk cavities, rotor or stator internal cooling flow/external flow interaction, etc. The combination of an unstructured or semistructured grid solution procedure with an adaptive grid technique provides an intelligent means of evolving the computational grid and, thus, the accuracy of the flowfield solution over complex domains in a most efficientmanner. The development of such a procedure for viscous flows has been the primary goal of the effort to be described in this paper.

The basic approach of the adaptive embedded solution procedure described herein is based upon the adaptive Euler technique developed previously by Dannenhoffer.[7] In the current work, the Reynolds-averaged Navier-Stokes equations are integrated to steady state on successively refined grids until solutions on successive grids are "close" to each other. The embedded grids are generated by employing a fixed global grid and automatically subdividing the computational cells in the immediate vicinity of pertinent flow features. These flow features, such as stagnation points, shocks, and viscous layers, are located through the use of velocity difference and vorticity refinement parameters. The integration procedure used to solve the Navier-Stokes equations consists of the time marching control volume scheme developed by Davis et al.[8,9] A generalization of Ni's multiple-grid method[10] is used both for increasing the overall convergence rate, as well as to couple the solutions on the various embedded grids. When applied to isolated airfoil or cascade calculations, this scheme yields solutions that are as accurate as globally refined solutions, but require at least an order-of-magnitude less computing resources over a wide range of flow conditions.

Since the current work is an extension of the previously published cascade Navier-Stokes[8-10] and adaptive grid embedding[7,11,12] procedures, this paper will only briefly review the numerical techniques used in these procedures and will focus on describing the details of the new techniques necessary for viscous adaptive grid embedding solutions in turbomachinery cascades. Results will then be shown for a wide range of axial turbomachinery cascade configurations, including a transonic turbine, a transonic positive-incidence stalled compressor and a transonic fan as a demonstration of the accuracy and efficiency of the current procedure.

Flow Integration Procedure

The quasi-three-dimensional Navier-Stokes equations are solved in conservation form in the blade relative frame. Streamtube contraction and radius change effects are included in the governing equations to accurately simulate the flow through cascade passages.

An explicit, time-marching, control volume, multiple-grid procedure[8,10] is used to iteratively solve the Navier-Stokes equations in pseudotime until a steady-state solution is obtained. In this procedure, the governing equations are integrated around nonoverlapping cells to give the cell center time rate changes of the primary variables. These cell center time rate changes are subsequently distributed to the computational nodes, using a distribution formula developed by Ni.[10] This

Presented as Paper 89-0204 at the 27th Aerospace Sciences Meeting, Reno, NV, Jan. 9-12, 1989; received Jan. 30, 1989; revision received March 15, 1990.

*Senior Research Engineer. Member AIAA.

formula consists of an equidistribution of the cell center time rate changes plus a windward biasing term that provides for second-order accuracy in time and space on uniform meshes. Upon updating the primary variables in time, a generalization of the Ni multiple-grid scheme is used to accelerate convergence to steady-state and to couple the solutions of the various embedded meshes. Since the elements of the distribution formula are calculated exclusively from information contained within a given cell, this numerical approach lends itself very well to the current unstructured adaptive grid embedding approach.

At the upstream boundary of the cascade passage, the relative stagnation pressure, stagnation temperature, and gas angle are held fixed. The average static pressure is held fixed at the exit boundary, when the flow component normal to the boundary is subsonic. When the normal flow component at the exit boundary is supersonic, a radiation (or extrapolation) condition is imposed. At solid boundaries, the velocity tangency condition is imposed for inviscid flows and for viscous flows, the velocity components are set to zero and a prescribed wall temperature or heat flux distribution is held fixed. Because of the unstructured mesh and associated data structure used, the periodicity condition for cascades is automatically satisfied by having the cells that lie immediately above and below the periodic line reference the same nodal locations. Thus, upon distributing the cell center time rate changes to the computational nodes, using the Ni[10] distribution formula, the nodes that lie along the periodic line receive contributions from all of its surrounding cells. In this way, the nodes along the periodic line are indistinguishable from any other interior node in the computational domain and, hence, no boundary condition application is required.

In order to capture shocks and eliminate oscillations in the flowfield in regions of coarse grid spacing, a numerical smoothing model is included in the present approach. A combination of second- and fourth-difference numerical smoothing operators[8] is added to the right-hand side of the numerical approximation of the Navier-Stokes equations. Second differences of the primary variables are obtained in the current unstructured grid procedure by collecting the first differences across the faces of the computational cells surrounding a given node. Fourth differences are calculated by taking two consecutive second differences. The second- and fourth-difference numerical smoothing of the primary variables along the computational grid lines normal to the boundaries is set to zero at the boundary nodes, and, for viscous flows, the numerical smoothing of the velocity-based primary variables is reduced to zero through the boundary layer in order not to contaminate the viscous flow solution. The numerical smoothing in the wake region of cascades is performed consistently with the interior domain. The nominal smoothing used in this region is adequate to eliminate unsteady trailing edge shedding phenomena and stabilize the flow so that a steady-state solution can be obtained.

The Baldwin-Lomax[13] two-layer algebraic turbulence model has been implemented into the present adaptive grid procedure to calculate the turbulent viscosity coefficient. Although implementation of the Baldwin-Lomax algebraic turbulence model is somewhat complicated within an unstructured grid solution procedure, it has been chosen over differential equation turbulence models, such as the $k-\epsilon$ model, for the current procedure primarily because of its efficiency.

In the present approach, the Baldwin-Lomax turbulence model has been implemented along the tangential lines of the initial computational grid, which lie nearly normal to the solid surface. Corrections are made to the distance calculations along the tangential computational lines and the velocity field to account for the difference between the true body normal and the tangential computational lines. Since the current adaptive grid procedure begins with an initial structured-like grid for cascade applications, implementation of the Baldwin-Lomax turbulence model along the tangential lines of this grid is relatively straightforward.

The semistructured nature of the current adaptive grid approach and the fact that rectangles are used in this approach rather than triangles allow for simple application of the algebraic turbulence model without the need for special body-oriented zonal grids. In addition, these features allow for straightforward application of the Ni[10] multiple-grid scheme to accelerate convergence and communicate between the different embedded meshes. Also, with the current approach, the Klebanoff intermittency function in the outer region of the boundary layer can be used to allow for a smooth decay of the eddy viscosity, which eliminates the need to zero out the eddy viscosity at some predetermined distance from the airfoil surface.

Upon adaptation of the grid, computational nodes are generated at stations that lie between the streamwise stations of the initial computational or turbulence model grid. In the present scheme, the eddy viscosity at these intermediate nodes is calculated using values of the normal distance, velocity, and vorticity based Baldwin-Lomax variables that are interpolated from information contained along the initial tangential grid lines using bilinear interpolation. The Baldwin-Lomax inner and outer layer formulas are subsequently used to calculate the eddy viscosity distribution at the intermediate nodes directly. This technique eliminates errors involved with interpolating the nonlinear eddy viscosity distribution at the intermediate nodes.

The additional nodes created from the adaptation process that lie along the initial tangential grid lines are included in the application of the turbulence model after each adaptation. Thus, the number of tangential grid nodes used to apply the Baldwin-Lomax turbulence model at each streamwise station of the initial grid varies, depending upon the local amount of grid embedding. In this manner, the adaptation process not only serves to increase resolution of gradients in regions of flow features, such as the viscous layer, but also to increase the accuracy of the turbulence model as the solution evolves from that of the coarse initial grid to that of the final adapted grid.

Adaptation Procedure

The adaptation process used here is essentially the same as that used for the Euler computations of Ref. 7. The Navier-Stokes equations are iterated in pseudotime until steady state has been obtained on the current computational mesh. At that point, pertinent flow features are located throughout the domain and the computational cells in the immediate vicinity of these features are subdivided into four subcells to increase the resolution. Simultaneously, previously subdivided cells are fused away from the features, thereby deleting unnecessary resolution. The flow solution procedure then continues on the newly formed mesh. Extension of the current cell division scheme to allow for directional adaptation, such as that suggested by Kallinderis and Baron,[14] in which the computational cells can be divided into halves in either direction, should be straightforward and is planned for the future. As described in Ref. 15, the entire adaptation process is controlled by a hybrid expert system.

The process of locating appropriate features in the flowfield is accomplished by first scanning the entire domain and computing some refinement parameter. The refinement parameters are then normalized and a threshold is automatically chosen such that any node whose refinement parameter exceeds the threshold value is determined to be part of a feature.

The essential difference between feature detection for inviscid and viscous computations lies in the definition of the refinement parameters. For inviscid transonic flows, the first difference of density was found to be a suitable refinement parameter for locating shocks, slip lines, and expansion wave regions.[7] However, for viscous flows, different refinement parameters are required to detect the viscous flow features present. In the current work, it was found that two independent refinement parameters, the first difference of the velocity

and vorticity, are suitable choices. The velocity difference across the faces of the computational cell has been found to be a good parameter to locate inviscid phenomena, such as stagnation points, shocks, and expansion waves. The velocity difference parameter is somewhat more conservative, providing slightly more embedded cells for a given flow than would be defined using the density difference. In addition, the velocity difference was found to be useful for locating stagnation points in low-speed applications and provides a good initial marker for defining the extent of viscous layers, including boundary layers, shear layers, and wakes. The velocity difference parameter was not found to be sufficient, however, to track and completely encompass the viscous layers. For these viscous features, the vorticity magnitude was found to be a very good parameter to define the extent of the high velocity gradient, viscous regions. Other refinement parameters, such as vorticity difference and total pressure loss, were investigated but were found to give results that were not as good as those obtained with the velocity difference and vorticity magnitude.

Results

The previously described adaptive grid Navier-Stokes procedure has been validated on several model problems. Solutions for these model problems have shown excellent agreement with boundary-layer calculations, experimental data, and other Navier-Stokes analyses.[8,16] The present procedure has been applied to several cascade configurations operating over a wide range of flow conditions. Solutions for a transonic turbine, a positive incidence stalled transonic compressor, and a transonic fan will be shown here as a demonstration of the capability to compute complex flows within quasi-three-dimensional turbomachinery cascades.

In all of the viscous calculations shown below, the temperature on the surface of the airfoil was held constant at the freestream total temperature, and the flow was assumed to be fully turbulent. Two levels of multiple-grid coarser than the initial grid were used in each solution to further accelerate convergence. All of the solutions were adapted to grids five levels finer than the initial grid. Solutions were considered converged when the maximum change in the total mass flux, ρV, was less than 5×10^{-4} for each refinement level.

For a viscous calculation, the initial computational grid consists of a periodic C grid, with 97 points in the streamwise direction and 13 points stretched in the tangential direction. The periodic C grid is constructed using a Poisson solution procedure, as described in Ref. 8. Upon adaptation, the first grid point off the body in the viscous calculations is located at a distance of 5×10^{-5} of the axial chord away from the surface. For an inviscid calculation, the initial computational grid consists of a periodic C grid with 97 streamwise and 9 evenly distributed tangential points.

The present adaptive grid approach has been found to greatly reduce computational time and storage when compared to fixed structured grid calculations that use grid spacing comparable to that within the fine grid region of the adaptive grid approach throughout the entire domain. For a fixed structured grid calculation of complex flows, such as those shown below with shocks and separated regions of unknown location, a globally fine grid with spacing equal to that of the fine grid region of the adapted grid procedure would be required to obtain comparable solution accuracy to that of the adaptive grid approach. Consequently, the adaptive grid embedding procedure requires an order-of-magnitude less computational time and storage than the globally fine fixed grid procedure. Also, the total amount of computational time used during a series of multiple-pass calculations, in which the computational grid is interactively refined by the user to obtain a grid independent solution, is significantly greater than the computational time required for one adaptive grid calculation.

The adapted computational grids for the cascade geometries presented have been refined much further than would be typically required for common engineering purposes, primarily as a demonstration of the capabilities of the current approach. Since the desired accuracy level is specified by the user, solutions can be obtained with more or less refinement than the cases shown here.

The solutions presented below used from 11,000 (inviscid) to 50,000 (viscous) grid points in the final adapted grids. The computational grids for these cases typically doubled in size after each level of refinement. This rate of growth in computational nodes between refinement levels can be controlled in the present adaptive grid approach through the definition of the threshold level in the cell division scheme. Calculations typically required 200 iterations for inviscid flows or 300 iterations for viscous flows to reach a steady-state solution for each refinement level. These solutions were executed on an Alliant FX-8 vector/parallel mini-supercomputer in which five central processing units work together concurrently on a given computation. Optimization of the adaptive grid Navier-Stokes code has been performed by the Alliant compiler, which vectorizes inner DO-loops and parallelizes outer DO-loops. In addition, a cell-based coloring scheme has been incorporated into the adaptive grid procedure to allow efficient parallelization. This coloring scheme essentially sorts the computational cells such that adjacent cells always belong to separate groups (or colors). This strategy is required in order to vector/parallel the flow solution procedure flux balance and distribution operations. Computations took on the average 4.0×10^{-4} s/node/iteration for an inviscid calculation and 1.3×10^{-3} s/node/iteration for a viscous calculation. For the same total number of computational nodes and convergence levels, the present adaptive grid procedure took approximately the same amount of computational time as the fixed structured grid Navier-Stokes procedure described in Ref. 8 for the solutions presented here.

Transonic Turbine Cascade

Inviscid and viscous calculations have been performed for a transonic turbine reported by Kopper et al.[17] The aerodynamic conditions, including the inlet and exit Mach numbers M_1 and M_2, the gas angles β_1 and β_2 (measured from axial), along with the streamtube contraction H_2/H_1, and inlet unit Reynolds number Re_1, chosen for the adaptive grid calculations for the transonic turbine cascade are given in Fig. 4.

Figure 1 shows the final adapted computational grid for a viscous calculation and the corresponding predicted numerical schlieren,[18] which was generated from gray-scale solid contours of the function, $\ln(\rho)|\nabla \cdot V|$. This numerical schlieren along with an experimental schlieren presented in Fig. 2 show the predicted expansion wave/shock system at the trailing edge and throat regions of the cascade very well. Similar plots of Mach number contours have not been found to demonstrate these features of the flow as well as the numerical schlieren for this case, since the expansion wave/shock system is oblique relative to the flow direction. Figure 1 shows that the adaptive grid procedure has automatically located and embedded a fine grid at the leading edge around the stagnation point, in the throat region between the blades, and around the trailing-edge expansion wave/shock system. In addition, the adaptive grid scheme has also embedded a fine grid in the boundary layer adjacent to the airfoil surface and in the wake region.

As shown in Figs. 1 and 2, expansion waves that originate at the trailing edge tangency points are generated as the flow expands around the trailing edge into the near wake immediately behind the trailing edge. The flow, upon over-expanding around the trailing edge, shocks at the end of the near wake where the suction and pressure side flows meet. The oblique shock emanating from the suction side of the near wake passes into the exit freestream flow at a relatively sharp angle. The shock originating from the pressure side of the near wake,

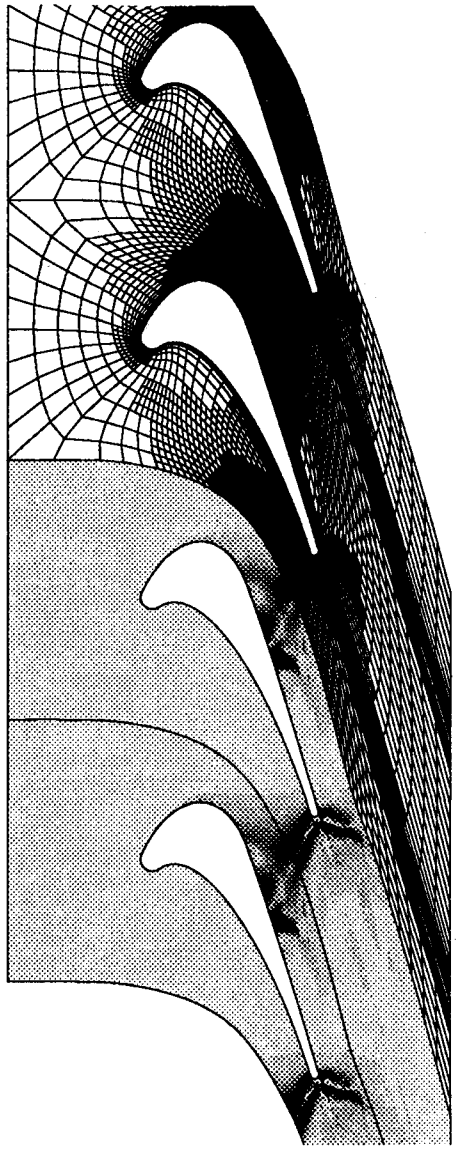

Fig. 1 Adapted viscous computational grid and numerical schlieren for transonic turbine cascade.

however, traverses across the passage, where it strikes the suction side of the adjacent turbine blade near 60% axial chord and is reflected into the exit freestream.

The ability to locate pertinent flow phenomena such as those located at the trailing edge of the transonic turbine blade and increase the local resolution of the solution to a prescribed level of accuracy is a very important feature of the current adaptive grid Navier-Stokes approach. The transonic turbine trailing-edge flow exhibits many types of fluid dynamic phenomena, including the expansion waves, shocks, boundary layers, shear layers, wakes, and near wake recirculation region. Figure 3 shows the evolution of the computational grid in the turbine trailing edge region from the initial grid to the final adapted grid with five levels of refinement. Comparison of the grids shown in this figure demonstrates the ability of the current procedure to locate and resolve the different phenomena occurring in this region. This is especially important in order to accurately predict the airfoil loading and performance for this case, since the flow in this region determines the shock structure, the pressure distribution, and the trailing-edge base pressure.

The adapted computational grid and the resulting flowfield of an inviscid calculation for this turbine cascade is very similar to that shown in Fig. 1, except for the fine grid embedded adjacent to the blade surface and in the wake. The predicted

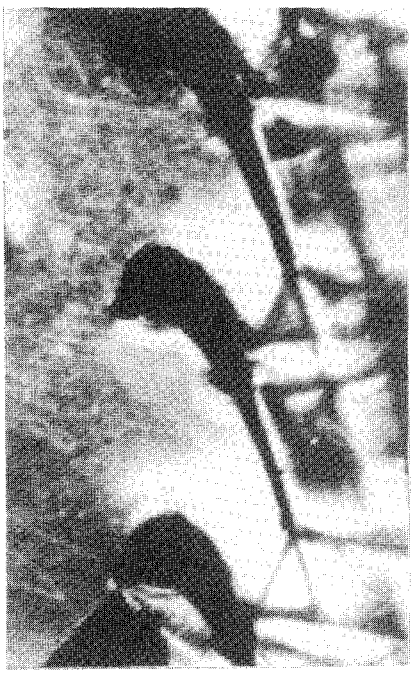

Fig. 2 Experimental schlieren for transonic turbine cascade.

shock structure for the inviscid calculation is much like that of the viscous solution. For inviscid flows, it is advantageous to model the trailing-edge flow region using a wedged trailing-edge shape to eliminate trailing-edge stagnation point regions and to reduce numerical losses. For transonic turbines, however, the shape of the wedge can be critical in the determination of the flow solution since the expansion wave/shock structure is directly related to the wedge shape.

The evolution of the predicted viscous adaptive grid pressure distribution is shown in Fig. 4, along with the experimental data. This figure shows how the solution changes from that of the coarse initial grid (distribution-0) to that of the final grid (distribution-5). The differences in the predicted pressure distributions become smaller between consecutive refinement levels as the final solution is approached. Good agreement exists between the final predicted solution and the experimental data. The base pressure predicted by the viscous calculation is in very good agreement with the experimental base pressure measurement. This represents an important capability since the base drag penalty in a transonic turbine can account for a significant portion of the overall total pressure loss through the cascade passage. The ability of a Navier-Stokes procedure to accurately predict the base pressure for transonic turbine cascades is a major accomplishment that is now feasible using the adaptive grid technology of the current approach.

Figure 5 shows the evolution of the skin friction distribution of the initial grid (0) and five refinement levels. In addition, this figure shows the predicted skin friction distribution from a direct boundary-layer analysis,[19] using the predicted pressure distribution of the viscous adaptive grid solution as the prescribed-edge boundary condition. Figure 5 shows that the predicted skin friction distribution of the adaptive grid procedure converges, and that the final solution is in very good agreement with the boundary-layer solution. Also, good agreement exists between the predicted adaptive grid Navier-Stokes and boundary-layer separation location on the suction side of the blade, which is caused by the trailing edge shock.

The mass averaged exit total pressure loss coefficient, $(P_{T_1} - P_{T_2})/P_{T_1}$, and exit gas angle β_2 predicted by the adaptive grid Navier-Stokes procedure for this transonic turbine cascade were 0.043 and -73.9 deg, as compared to the experimental values of 0.044 and -75.7 deg. Excellent agreement exists between the predicted and experimental total

pressure loss, whereas a small discrepancy exists between the predicted and experimental exit gas angle that can be attributed to the modeling of the quasi-three-dimensional streamtube contraction[9] in the analysis.

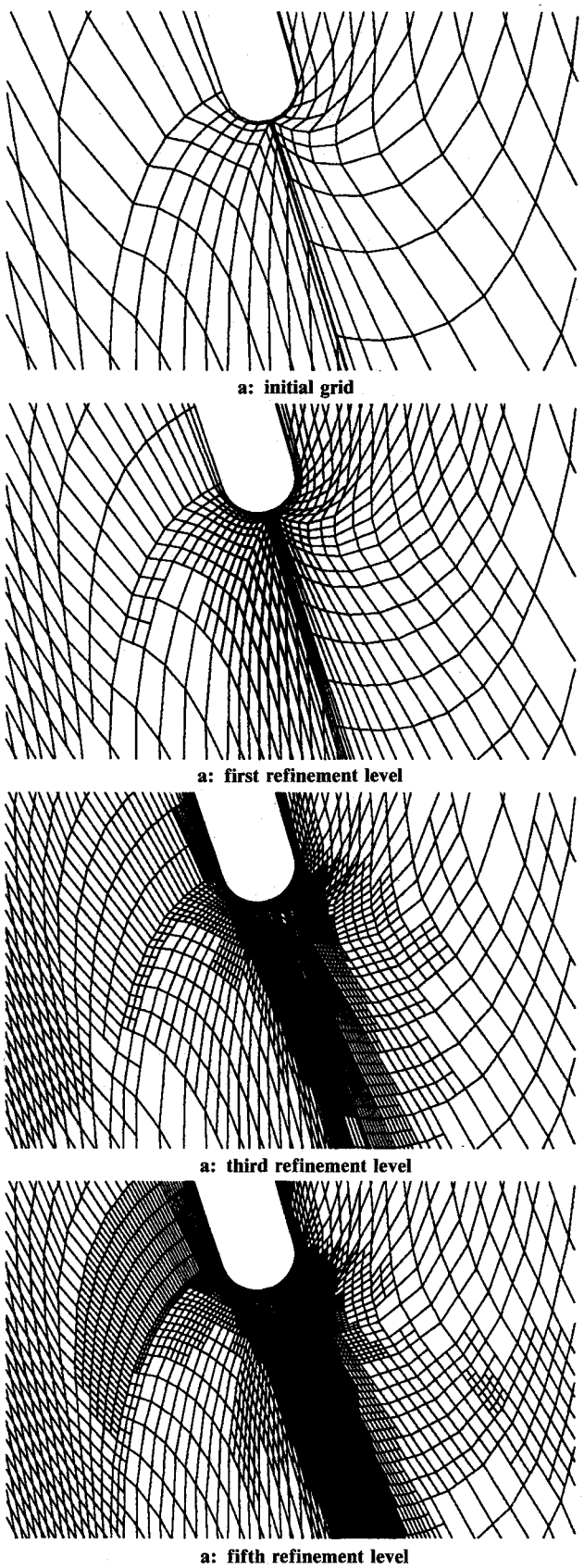

Fig. 3 Evolution of computational grid at trailing edge of transonic turbine cascade.

Transonic Compressor Cascade

An area in which adaptive grid schemes are very useful is in the calculation of stalled flows over compressor cascades. As demonstrated in Ref. 9, the boundary layer on a stalled airfoil can lift off the surface, out of the region of the fine grid in a fixed nonadaptive grid procedure, leading to solutions in which the resolution of the shear layer may be inadequate. Adaptation and refinement are required to maintain a fine computational grid around the shear layer in the separated flow region. A demonstration of the current procedure to track separated flows is shown here for a transonic compressor, reported by Stephens and Hobbs,[20] at a positive 7 deg incidence. The aerodynamic conditions for these computations are given in Fig. 8.

Figures 6 and 7 show the final adapted computational grid for the viscous flow calculation at this incidence. For this case, separation occurred over the aft 50% of the airfoil suction surface, which is in good agreement with the solution presented in Ref. 9 and the experimental data. A fine computational grid has been embedded around the stagnation point region, around the suction side shock, adjacent to the airfoil through the boundary layer, and within the wake. In addition, the shear layer at the edge of the reversed flow region on the suction side of the airfoil has been tracked and a fine embedded grid has been placed around the high-gradient region, as demonstrated in Fig. 7. This capability of automatically locating and refining the computational grid around the different features in the flow eliminates the need for user interaction with the computational mesh and corresponding multiple-pass calculations in order to achieve grid independent solutions.

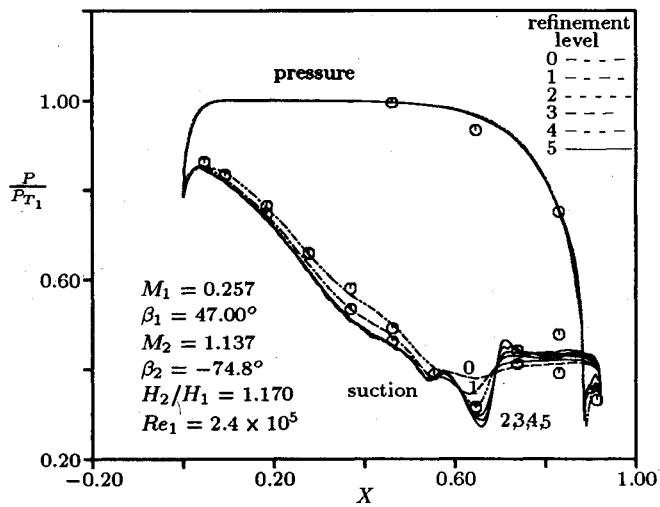

Fig. 4 Pressure distribution for transonic turbine cascade (lines—Navier-Stokes, ⊙ —experiment).

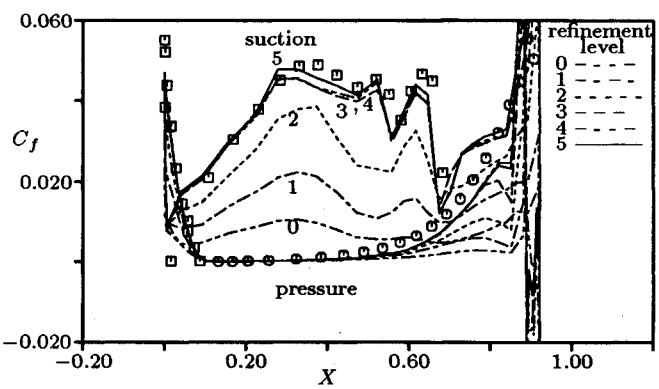

Fig. 5 Predicted skin friction distribution for transonic turbine cascade (lines—Navier-Stokes; ⊙, □ —boundary layer).

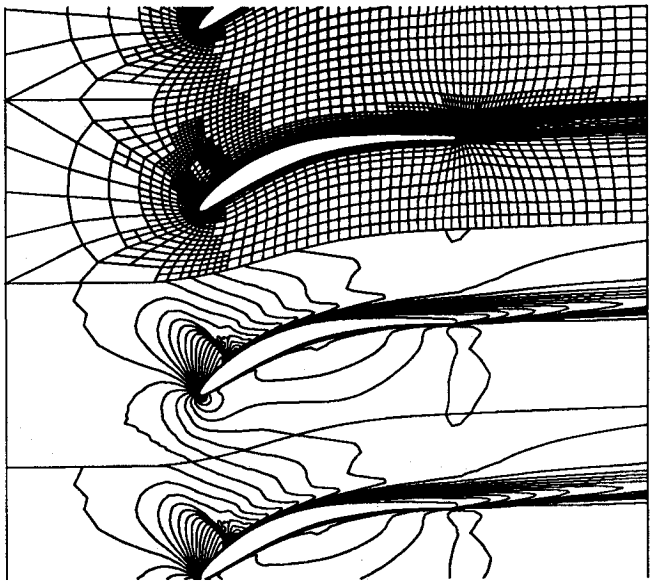

Fig. 6 Adapted viscous computational grid and Mach number contours for transonic compressor cascade ($M_{inc} = 0.05$).

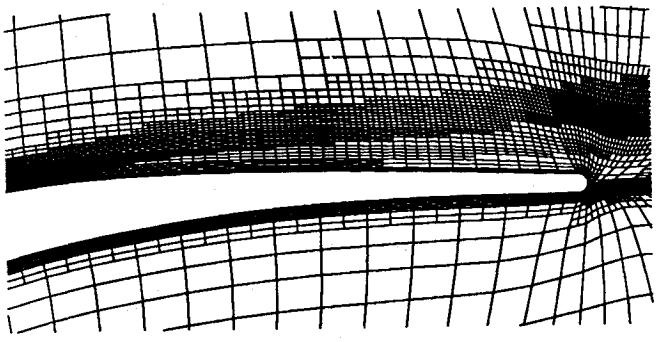

Fig. 7 Adapted viscous computational grid in separated flow region of transonic compressor cascade.

The Mach number contours, presented in Fig. 6 with increment $M_{inc} = 0.05$, show that the shock definition on the suction side of the airfoil is very sharp. Compared to the corresponding inviscid solution, the shock is weaker in strength and has moved slightly forward towards the leading edge. The Mach number contours also show the extent of the shear layer, as the flow separates off the suction surface, and indicate the thickness of the wake relative to the trailing-edge thickness.

The predicted inviscid and viscous pressure distributions for the transonic compressor at the 7-deg incidence stall point is shown in Fig. 8, in comparison with the experimental data. Good agreement exists between the predicted viscous solution and the experimental data for the pressure side of the airfoil. Differences exist between the viscous prediction and the experimental data on the suction side of the airfoil, however. These differences are probably due to the modeling of the quasi-three-dimensional streamtube contraction effects and the turbulence model for the separated flow region, as discussed in Ref. 9. The inviscid solution shows a strong, sharp rise in the pressure associated with the predicted shock, which is weaker in the viscous solution and experimental data. The significant difference between the inviscid and viscous predictions demonstrates the strong interaction that occurs between the shock and the viscous layer and shows the importance of including the viscous effects in solution procedures for transonic compressor cascades. The evolution of the predicted viscous pressure distribution from that of the initial grid to that of the final adapted grid with five levels of embedded grid is also shown in Fig. 8. This series of solutions shows a major

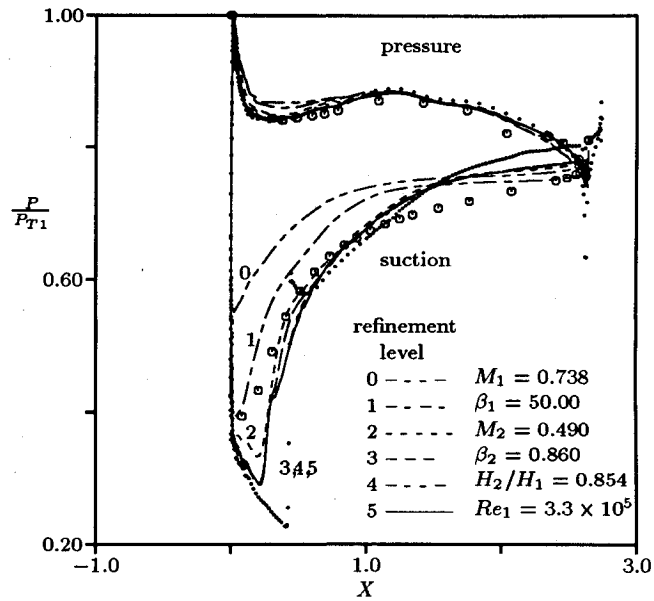

Fig. 8 Predicted pressure distributions for transonic compressor cascade (lines—Navier-Stokes, •••—Euler, ⊙—experiment).

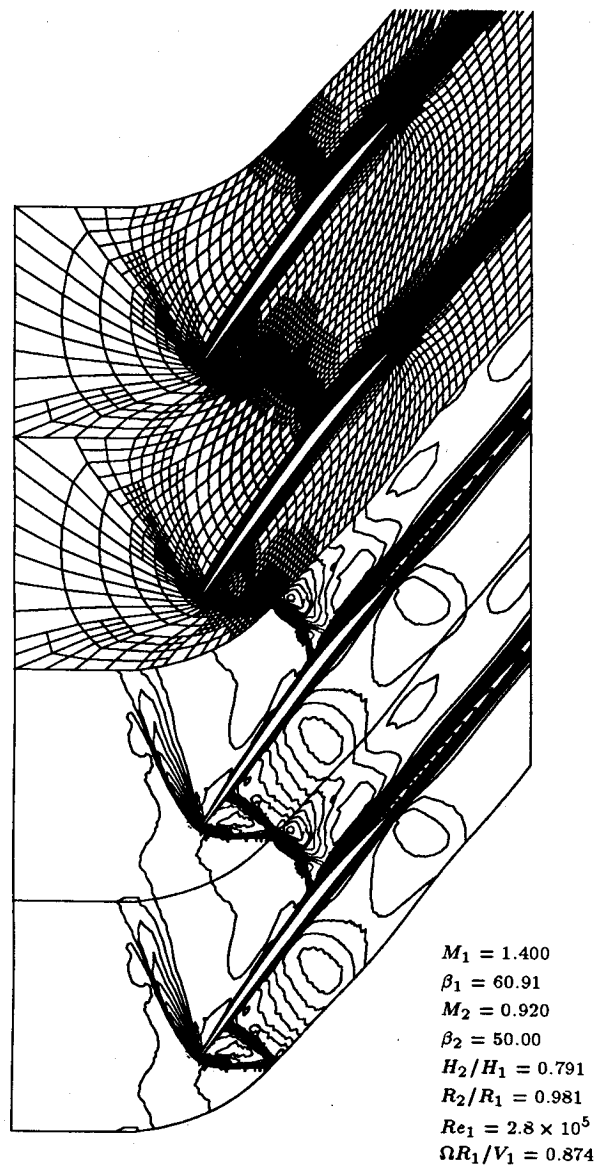

Fig. 9 Adapted viscous computational grid and Mach number contours for transonic fan ($M_{inc} = 0.05$).

difference between initial and final predictions and also shows the convergence of the pressure field to the final solution.

The predicted mass averaged exit total pressure loss coefficient, $(P_{T_1} - P_{T_2})/P_{T_1}$, and exit gas angle β_2 of the adaptive grid solution were 0.025 and 3.29 deg. These values are somewhat different from the experimental values of 0.046 and -0.85 deg, but are in good agreement with the fixed grid Navier-Stokes calculations of Ref. 9. The adaptive grid Navier-Stokes procedure has successfully predicted the large increase in exit total pressure loss at these stalled flow conditions compared to the total pressure loss at the design point, which was 0.006. The differences between the adaptive grid prediction and the experimental data for the predicted loss and exit angle are probably due to a breakdown in the quasi-three-dimensional streamtube contraction and turbulence modeling in the Navier-Stokes procedure, as well as to uncertainty in the experimental data for these stalled flow conditions.

Transonic Fan

The final test case to be shown is for a transonic compressor fan tested experimentally by Harvey and Hobbs.[21] In this test case, the effects of rotation, radius change, and streamtube contraction are all present. Laser velocimeter measurements were taken in the absolute frame of a rotating fan rig at several different radius locations. The fan section computed with the adaptive grid procedure corresponds to the 85% span location near the tip of the blade at the design point conditions given in Fig. 9, including the inlet to exit radius ratio, R_2/R_1, and the nondimensional wheel speed, $\Omega R_1/V_1$.

Figure 9 shows the final adapted grid for the viscous transonic fan calculation with the corresponding predicted Mach number contours. The experimental Mach number contours that were obtained from the experimental velocity measurements, using the assumption that the relative total temperature depends only on the radius (i.e., uniform rothalpy), are shown in Fig. 10. Very good agreement exists between the predicted and experimental shock structure and wake thickness. The adaptive grid procedure predicts a leading-edge bow shock and a normal shock that traverses across the entire passage from a position just behind the leading edge on the pressure side of the airfoil to the 60% axial chord location on the suction side of the adjacent airfoil. On the suction surface, the normal shock bifurcates into a lambda shock as it interacts with the boundary layer, causing separation of the flow over the remainder of the suction surface and a corresponding rapid increase in the boundary-layer thickness. The leading edge bow shock and passage normal shock merge near the midgap region, just behind the leading edge, causing a slip-line and corresponding indentation in the Mach number contours behind the shock intersection.

Figure 9 shows that the grid has automatically isolated the multiple shocks, as well as the different viscous layer regions,

Fig. 10 Experimental LDV Mach number contours for transonic fan.

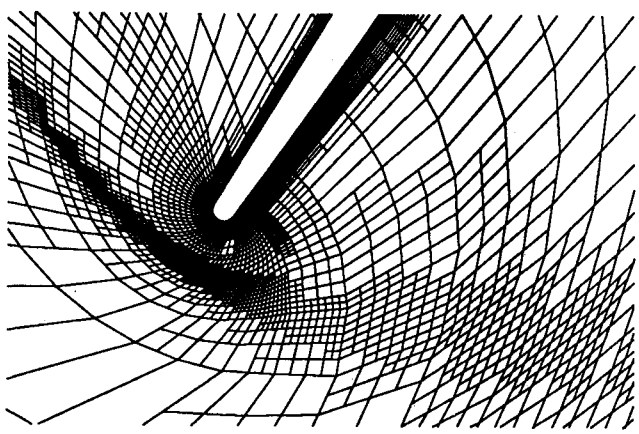

Fig. 11 Adapted viscous computational grid in leading-edge region of fan.

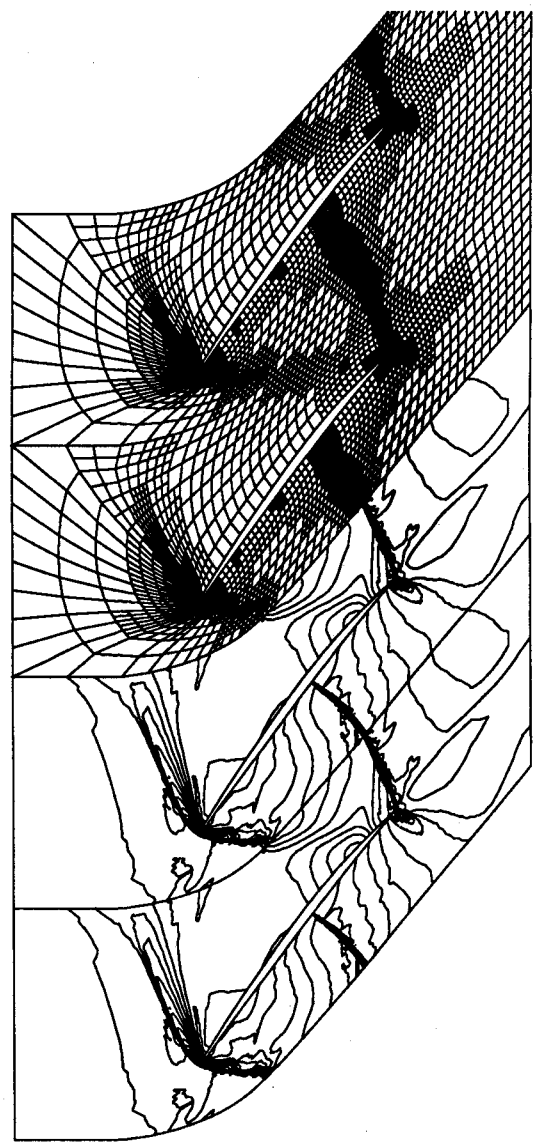

Fig. 12 Adapted inviscid computational grid and Mach number contours for transonic fan ($M_{inc} = 0.05$).

and has embedded a fine grid around these features. The final adapted grid in the leading-edge region of the fan blade is presented in Fig. 11. This figure shows the detail of the adapted grid around the leading-edge bow shock and boundary layer. This shock structure is very difficult to capture using a fixed structured grid procedure; and requires a very dense global grid to capture and define this shock system with the same detail that results from the adaptive grid procedure.

The predicted mass averaged exit total pressure loss coefficient, $(P_{T_1} - P_{T_2})/P_{T_1}$, and exit gas angle β_2 of the transonic fan adaptive grid solution were 0.095 and 50.36 deg, compared to the measured values of 0.098 and 50.0 deg. The very good agreement between the predicted and measured exit loss and angle demonstrates the ability of the present adaptive grid Navier-Stokes procedure to predict cascade performance for complex flows in transonic fans.

In a similar manner, as with the previous stalled compressor cascade, the adaptive grid scheme has also embedded a fine grid around the edge of the separated shear layer behind the shock just off of the suction surface of the fan. As will be further demonstrated with the corresponding inviscid calculation for this case, the capability of the present adaptive grid procedure to track the movement of the shocks in the fan passage caused by the shock/shock and shock/boundary-layer interactions and automatically refine the grids around the shocks and viscous layers gives designers, for the first time, a numerical tool to compute these complex flows that requires little or no user interaction.

The corresponding predicted inviscid solution for the transonic fan is shown in Fig. 12. The shock structure, shown in this figure, is very different compared to the viscous solution and experimental data. This result, which is typical of inviscid calculations for transonic fans, is a demonstration that the viscous effects are essential to establish the correct shock location and to properly model the actual flowfield. Once again, this figure demonstrates the ability of the adaptive grid procedure to track and place a fine grid around multiple shocks in the flow, which for this case include the leading-edge bow shock and the trailing edge normal shock.

Concluding Remarks

An adaptive grid embedding procedure has been developed for the computation of inviscid and viscous cascade flows. This procedure uses a strategy whereby the computational cells in the immediate vicinity of flow features, detected by the local vorticity magnitude and changes in velocity, are subdivided into four equal cells. The flowfield numerical procedure consists of an explicit time-marching control volume technique coupled to a multiple-grid procedure. Solutions are presented demonstrating the accuracy and efficiency of the procedure to automatically track and resolve complex inviscid and viscous quasi-three-dimensional cascade flows, including shocks, shock/boundary-layer interaction, separated flows, trailing-edge base flows, and wakes.

A major benefit of this effort has been that with an "intelligent" adaptive grid procedure, such as the grid embedding technique described here, computational grid independent solutions can now be obtained in an efficient manner for very complex flows with little or no user interaction. In addition, the current adaptive Navier-Stokes procedure can now be used to analyze and adequately model the physics of complex turbomachinery flows. With this capability in hand, the limiting factor for the present two-dimensional adaptive Navier-Stokes procedure is turbulence modeling, especially for separated flows. Further work is also necessary to make additional gains in computational efficiency for this Navier-Stokes method, so that it can be routinely used as a design procedure, as well as an analysis tool.

Acknowledgments

This work was supported by Pratt and Whitney and the United Technologies Research Center under the Corporate Research Program. The authors would especially like to thank H. D. Weingold and D. E. Hobbs of Pratt and Whitney for their help in this effort.

References

[1]Löhner, R., Morgan, K., and Zienkiewicz, O. C., "Adaptive Grid Refinement for the Compressible Euler Equations," *Accuracy Estimates and Adaptivity for Finite Elements,* Wiley, New York, 1984.

[2]Jameson, A., Baker, T. J., and Weatherill, N. P., "Calculation of Inviscid Transonic Flow Over a Complete Aircraft," AIAA Paper 86-0103, Jan. 1986.

[3]Holmes, D. G., Lamson, S. H., and Connell, S. D., "Quasi-3D Solutions for Transonic, Inviscid Flows by Adaptive Triangulation," American Society of Mechanical Engineers, Paper 88-GT-83, June 1988.

[4]Mavriplis, D., "Accurate Multigrid Solution of the Euler Equations on Unstructured and Adaptive Meshes," AIAA Paper 88-3706, July 1988.

[5]Shapiro, R. A., and Murman, E., "Adaptive Finite-Element Methods for the Euler Equations," AIAA Paper 88-0034, Jan. 1988.

[6]Berger, M. J., and Oliger, J., "Adaptive Mesh Refinement for Hyperbolic Partial Differential Equations," Manuscript NA-83-02, Stanford Univ., Stanford, CA, March 1983.

[7]Dannenhoffer, J. F., "Grid Adaptation for Complex Two-Dimensional Transonic Flows," ScD Thesis, Massachusetts Inst. of Tech., Cambridge, MA, Aug. 1987.

[8]Davis, R. L., Ni, R. H., and Carter, J. E., "Cascade Viscous Flow Analysis Using the Navier-Stokes Equations," *Journal of Propulsion and Power,* Vol. 3, No. 5, 1987, pp. 406–414.

[9]Davis, R. L., Hobbs, D. E., and Weingold, H. D., "Prediction of Compressor Cascade Performance Using a Navier-Stokes Technique," *ASME Journal of Turbomachinery,* Vol. 110, No. 4, Oct. 1988, pp. 520–531.

[10]Ni, R. H., "A Multiple Grid Scheme for Solving the Euler Equations," *AIAA Journal,* Vol. 20, Nov. 1982, pp. 1565–1571.

[11]Dannenhoffer, J. F., and Baron, J. R., "Robust Grid Adaptation for Complex Transonic Flows," AIAA Paper 86-0495, Jan. 1986.

[12]Dannenhoffer, J. F., and Baron, J. R., "Grid Adaptation for the 2-D Euler Equations," AIAA Paper 85-0484, Jan. 1985.

[13]Baldwin, B. S., and Lomax, H., "Thin-Layer Approximation and Algebraic Model for Separated Turbulent Flows," AIAA Paper 78-257, Jan. 1978.

[14]Kallinderis, K. G., and Baron, J. R., "Adaptation Methods for a New Navier-Stokes Algorithm," AIAA Paper 87-1167, June 1987.

[15]Dannenhoffer, J. F., and Baron, J. R., "A Hybrid Expert System for Complex CFD Problems," AIAA Paper 87-1111-CP, June 1987.

[16]Chima, R. V., "Analysis of Inviscid and Viscous Flows in Cascades with an Explicit Multiple-Grid Algorithm," *Journal of Propulsion and Power,* Vol. 3, No. 5, 1987, pp. 397–405

[17]Kopper, F. C., Davis, R. L., Milano, R., Dring, R. P., and Stoeffler, R. C., "High Pressure Turbine Supersonic Cascade Technology Report," NASA CR-165567 or PWA-5594-152, Nov. 1981.

[18]Whitfield, D., private communciation, 1988.

[19]Carter, J. E., "Inverse Boundary-Layer Theory and Comparison with Experiment," NASA TP-1208, Sept. 1978.

[20]Stephens, H. E., and Hobbs, D. E., "Design and Performance Evaluation of Supercritical Airfoils for Axial Flow Compressors," NAVAIR Rept. FR11455, June 1979.

[21]Harvey, W. B., and Hobbs, D. E., "Fan Aerodynamics from Laser Doppler Velocimetry," Pratt and Whitney Rept. 83-616-0028, Oct. 17, 1983.